The Photogrammetric Record 24(127): 217–245 (September 2009)

COMPARATIVE GEOMETRIC AND RADIOMETRIC EVALUATION OF MOBILE PHONE AND STILL VIDEO CAMERAS

DEVRIM AKCA (akca@geod.baug.ethz.ch)
ARMIN GRUEN (agruen@geod.baug.ethz.ch)
Swiss Federal Institute of Technology (ETH), Zurich

Abstract

This paper examines the potential of mobile phones to be used as front-end sensors for photogrammetric procedures and applications. For this purpose, two mobile phone cameras (Sony Ericsson K750i and Nokia N93) were calibrated over an indoor 3D testfield, using a self-calibrating bundle adjustment. Geometric accuracy tests were carried out in order to evaluate their metric performances and to compare the results with respect to two off-the-shelf digital still video cameras (Sony DSC W100 and Sony DSC F828). The geometric accuracy evaluation comprised an absolute accuracy test, JPEG test and temporal stability test. The radiometric capabilities of all cameras (except that the DSC W100 was replaced with a DSC T100 camera) were also evaluated and compared by carrying out modulation transfer function (MTF) analysis, image noise analysis and an operating range test. Substantial systematic errors were diagnosed in some systems. However, with proper calibration it is believed that these devices can be used for many photogrammetric tasks.

KEYWORDS: geometric accuracy, image noise, JPEG test, mobile phone cameras, modulation transfer function (MTF), operating range, self-calibration, temporal stability

INTRODUCTION

MOBILE MAPPING has been an issue within the geospatial community for some years. Through the use of moving platforms (terrestrial and aerial vehicles and more recently satellites) photogrammetry has from early times had a "mobile" component. Also, online and real-time processing is by no means new. However, with the availability of very affordable CCD/CMOS cameras with high (megapixel) resolution and other off-the-shelf devices, including compact computers (of the laptop type), the potential of building efficient mobile systems has increased substantially.

The use of an autonomous model helicopter for 3D modelling in different projects has already been reported (Lambers et al., 2007; Gruen, 2008). Location-based services and ubiquitous computing are current buzzwords of high societal visibility and relevance. Among various hardware and software components, mobile phones constitute an interesting option for image data acquisition and processing for obvious reasons: they are very inexpensive, light, portable and equipped with digital cameras and CPUs.

Laptops nowadays have so much processing power and storage capability that part of the 3D model generation work can be achieved immediately in the field. With available know-how and software modules in sequential estimation, semi-automated and automated triangulation, and surface model generation and texturing, a good basis exists to build a system for mobile, field-based primary data acquisition and model building. Interesting future possibilities are anticipated for online processing of acquired image data by mobile phone cameras. This opens the path for a paradigm shift from "Mobile Mapping" to "Mobile 3D Modelling".

This paper examines the potential use of mobile phones as a front-end sensor for photogrammetric procedures and applications.

Mobile Phone Cameras as Front-end Sensors

Mobile phone cameras have been brought into use for many applications in recent times. One of the most prominent applications is character/text recognition in a flexible and portable fashion (Watanabe et al., 2003; Koga et al., 2005; Parikh, 2005). Rohs (2004) reports on a scenario where camera phones are used to recognise the visual codes in the scene. By recognising a code tag, the device determines the code value, the targeted object or image element. The phone's wireless communication channel is used to retrieve online content related to the selected image area or to trigger actions based on the sensed code.

In a facial animation study for mobile phones, Riegel (2005) created a specific 2D head model using a generic 3D face model and portrait images. The model is animated via voice or text. Al-Baker et al. (2005) use a GPRS- and WAP-enabled "personal digital assistant" (PDA) or mobile phone for human face identification. The system allows the user to send an image of a human face, acquired through a mobile phone with a built-in camera, to perform automatic face recognition remotely. The user will then instantly receive details of the person, if a match is found. The system can be especially useful for instant face identification and authentication tasks.

Clemens et al. (2005) developed a panoramic image application suite for mobile phone cameras. The image stitching is carried out in real time. Pittore et al. (2005) implement an image-based context awareness engine specifically for archaeological sites and museums. Visitors can "ask" for information about an unknown monument by simply taking a picture of it with a camera-integrated mobile phone and sending it to the system for recognition. Ueda et al. (2004) use mobile phones, equipped with a camera and a GPS chip, as a content provider to a geographical information system (GIS). Users can annotate objects in the environment by sending text, picture and location information via mobile phone to a central database.

Chung et al. (2004) correct the radial lens distortion of a mobile phone camera, applying a calibration procedure from Lenz and Tsai (1988). However, their experiment lacks numerical results and analysis. In a recent study, Aydar et al. (2007) used mobile phone photographs to obtain rectified images of building façades.

In spite of the availability of a broad diversity of applications, at the time of writing studies on the metric capabilities and characteristics of mobile phone cameras have not yet been published.

In 2004, Sharp Corporation developed a 2 megapixel (Mpixel) CCD camera module with $2\times$ optical zoom and auto-focus function (Fig. 1(a)) intended for use in mobile phones (Physorg, 2004). In 2005, they released two new camera modules (Fig. 1(b)) with a 3 Mpixel CCD chip (Physorg, 2005). One year later, Samsung announced a 10 Mpixel camera phone (Fig. 1(c)) at the CeBIT exhibition in Hanover (Williams, 2006). These examples show the rapid progress in the technology of mobile phone cameras. When writing this paper, 8 Mpixel

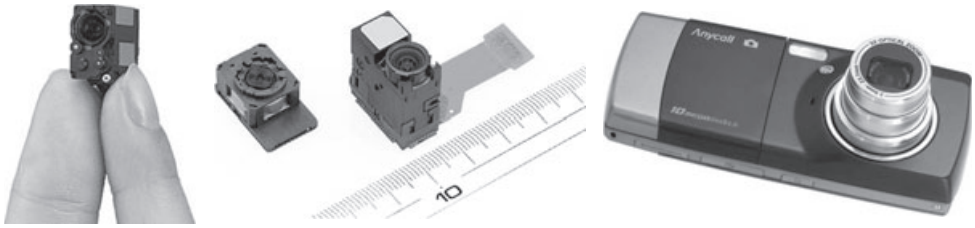

(a) (b) (c)

FIG. 1. (a) Sharp LZP0P-3738 2 Mpixel CCD camera module; (b) Sharp LZ0P-3751 and -3758 3 Mpixel CCD camera modules; (c) Samsung SCH-B600 10 Mpixel camera-integrated mobile phone.

mobile phone cameras (Nokia N86, Sony Ericsson C905, Samsung S8300) were already on the market.

Owing to their very limited size and restricted material and equipment costs, the production of mobile phone cameras is a challenge (Chowdhury et al., 2005; Myung-Jin, 2005). The impact of their production specifications on the stability of interior orientation and 3D object reconstruction capabilities has not yet been studied adequately.

Radiometric performance of an imaging system is also of concern. Many imaging sensors have been investigated: IKONOS (Baltsavias et al., 2001), OrbView-3 (Kohm, 2004), Cartosat-1 (Crespi et al., 2008), ADS40 (Pateraki and Baltsavias, 2002; Markelin et al., 2006), TLS (Zhang, 2005), DMC (Honkavaara et al., 2006) and various photogrammetric film scanners (Gruen, 1983; Baltsavias et al., 1998). Early work can be found in Brock (1968), Scott (1968), Welch (1971) and Welch and Halliday (1973).

This work investigates the metric and radiometric accuracy potential of two recent mobile phone cameras (Sony Ericsson K750i and Nokia N93) and compares them with three off-the-shelf digital still video cameras (Sony DSC W100, Sony DSC T100 and Sony DSC F828). These mobile phone and still video cameras vary in terms of sensors and image formats. The scope of these comparisons is to describe the metric and radiometric capabilities of the mobile phone cameras with respect to the state-of-the-art still video cameras using the same testfield under the same conditions. The differences between the various cameras in terms of image format (number of pixels) do not really matter because this can be compensated by a calculation factor. The preliminary results have been published in Gruen and Akca (2007; 2008a,b).

The next section introduces the cameras and the calibration/validation testfield and explains the geometric tests. In this section, the self-calibration, accuracy testing, JPEG testing, temporal stability testing (of the interior orientation over time) and image residual analysis are explained. The following section gives the results of the radiometric investigations, namely, modulation transfer function (MTF) analysis, image noise analysis and operating range analysis. A comparative evaluation of the results is presented in the last section of the paper.

GEOMETRIC PERFORMANCE TESTS

Cameras

Four cameras are used in the geometric evaluation (Fig. 2). Two of them are mobile phone cameras (Sony Ericsson K750i and Nokia N93) and two are off-the-shelf digital still video

(a) (b) (c) (d)

FIG. 2. Cameras used in the tests:
(a) Sony Ericsson K750i; (b) Nokia N93; (c) Sony DSC W100; (d) Sony DSC F828.

TABLE I. Technical specifications of the cameras.

	K750i	*N93*	*W100*	*F828*
Sensor type	CMOS	CMOS	CCD	CCD
Sensor size	4·5 mm × 3·4 mm	4·5 mm × 3·4 mm	7·2 mm × 5·3 mm	8·8 mm × 6·6 mm
Pixel size	2·8 μm	2·2 μm	2·2 μm	2·7 μm
Image format	1632 × 1224	2048 × 1536	3264 × 2448	3264 × 2448
	2 Mpixel	3·2 Mpixel	8 Mpixel	8 Mpixel
Lens	Unknown	Carl Zeiss	Carl Zeiss	Carl Zeiss T*
		Vario-Tessar	Vario-Tessar	Vario-Sonnar
Focal length	4·8 mm	4·5 to 12·4 mm	7·9 to 23·7 mm	7·1 to 51·0 mm
Optical zoom	No	3×	3×	7×
Auto focus	Yes	Yes	Yes	Yes
Aperture	f/2·8 (fixed)	f/2·8 (fixed)	f/2·8 to 5·2	f/2·0 to 8·0
Output format	JPEG only	JPEG only	JPEG only	JPEG and TIFF

cameras (Sony DSC W100 and Sony DSC F828). The mobile phone cameras have CMOS sensors of a smaller size than the CCD chips in the off-the-shelf cameras, and smaller lenses. The technical specifications of the four cameras are given in Table I.

Testfield

The photogrammetric 3D calibration field at the Institute of Geodesy and Photogrammetry at ETH Zurich was used. It is 3·4 m × 2·0 m × 1·0 m in size. The room has stable temperature (22°C) and humidity (40%) by means of air conditioning. The 3D coordinates of 87 well-distributed control points (GCP) were measured using a Leica Axyz system. The Leica Axyz system consists of two Leica total stations (TC 3000 and TC 2002) and one processing computer unit connected to them (Fig. 3). After an initialisation step, two operators simultaneously measure the vertical angles and horizontal directions to the targeted points. The system calculates the 3D coordinates (by spatial intersection) and the precision values in real time. The scale of the object space was given by measuring a bar whose length was accurately defined by interferometry as 1000·051 ± 0·010 mm. The average theoretical precision values of the GCPs are ±0·03, ±0·05 and ±0·03 mm for the X, Y and Z axes, respectively.

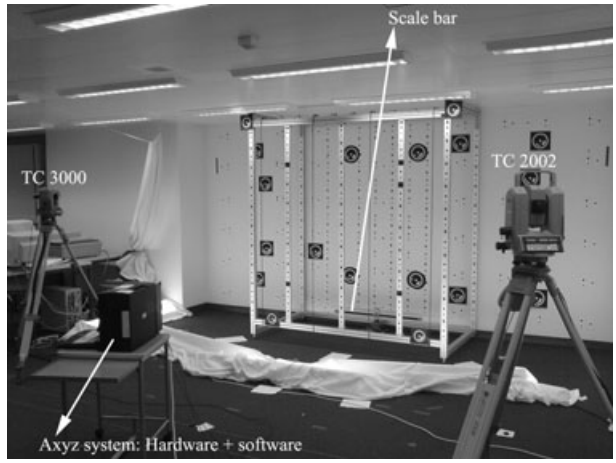

FIG. 3. The 3D testfield and the Axyz system. Note that the picture was taken by the K750i camera.

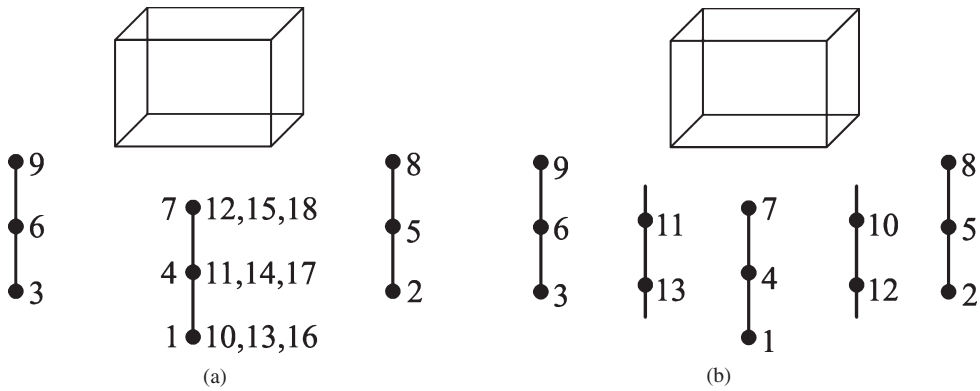

FIG. 4. (a) Image acquisition geometry for the calibration of the K750i, and (b) for the N93, W100 and F828. Black circles stand for the image stations and the wired cubes represent the 3D testfield.

Imaging Configuration

For the calibration of the K750i, 18 images from three locations (each of which has three stations, down, middle and up) were taken in a convergent geometry mode (Fig. 4(a)). Nine images were taken in normal mode (images 1 to 9) and three each of the remaining nine images are rotated −90° (images 10 to 12), +90° (images 13 to 15) and 180° (images 16 to 18), respectively.

For the calibration of the N93, W100 and F828 cameras, an image acquisition geometry with 13 images (Fig. 4(b)) was used. Images 1 to 9 are in normal mode and 10 to 13 are rotated. However, different rotated image versions were used. For camera N93, images 10 and 11 were rotated −90° and images 12 and 13 were rotated +90°; for camera W100, images 10 to 13 were all rotated +90°; and for camera F828, images 11 and 13

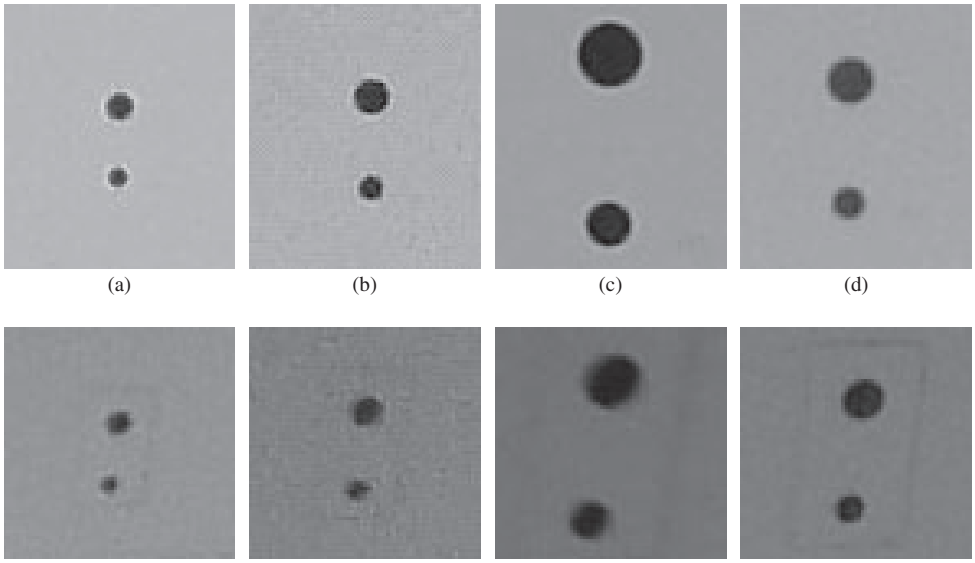

FIG. 5. Image quality of the cameras. (a), (b), (c) and (d) are cropped images at station 4 from the K750i, N93, W100 and F828, respectively. The two signalised points are approximately located at the centre of the image. The images (a), (b), (c) and (d) are 71×81 pixels in size. (e), (f), (g) and (h) are cropped images at station 1 from the K750i, N93, W100 and F828, respectively. The two signalised points are approximately located at the upper left part of the full image. The images (e), (f), (g) and (h) are 71×71 pixels in size.

were rotated $-90°$ and images 10 and 12 were rotated $+90°$. For N93, W100 and F828, the focal length was set to the smallest possible value by zooming and the focus was set to infinity.

The image measurements were performed with least squares template matching (Gruen, 1985) using the BAAP software developed in-house. Another in-house software package, SGAP (Beyer, 1992), was used for the bundle block adjustment with self-calibration.

The imaging quality differs between the cameras. In Fig. 5(a), (b) and (c), low-level image enhancement effects are strongly visible at the edges of the points. On the N93 images (Fig. 5(b) and (f)), strong JPEG artefacts are visible (Fig. 6). The F828 has the best visual overall image quality considering all images from all stations.

The K750i, N93 and W100 have only the JPEG output option. Their image measurements were carried out on their original JPEG images. The F828 can synchronously record both the JPEG and TIFF images for each scene. In the F828 tests, the original JPEG images were used for the absolute accuracy test and temporal stability test, while the TIFF images were used for the JPEG test.

Absolute Accuracy Test of the K750i

The 18 images version gives an a posteriori σ_0 value of about half a pixel (version 10 in Table II) and highly systematic residual patterns in some images (Fig. 7(a) and (b)), even after self-calibrating bundle adjustment with block-invariant additional parameters.

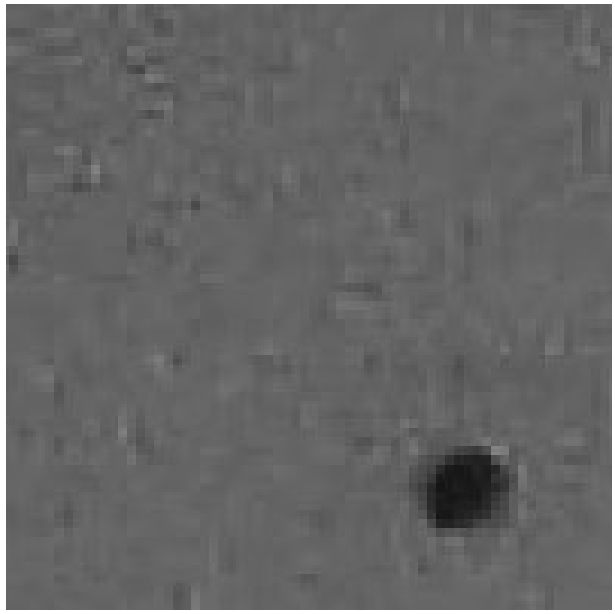

FIG. 6. 3 × zoom-in of the upper left part of Fig. 5(f). JPEG artefacts are visible.

The six most deteriorated images among the rotated ones were then excluded (images 11, 12, 13, 14, 16 and 18). Versions 11, 12, 13 and 14 in Table II give better σ_0 and precision values. However, a systematic pattern in the image coordinate residuals still remains, varying from image to image. Note that version 14 stands for the free network adjustment.

After Brown's 10 additional parameter (AP) set, Gruen's 44 AP set was applied (Grün, 1978). The block-invariant 44 additional parameters did not compensate for the systematic errors either (version 12).

Absolute Accuracy Test of the N93

The accuracy test of the N93, also based on block-invariant additional parameters, apparently gives better results. The σ_0 is a quarter of a pixel. A systematic error pattern still remains in the residuals (Fig. 7(c) and (d)); however, the magnitude is much less than in the K750i case. It has clearly achieved sub-millimetre accuracy in object space (version 23 in Table II) in all coordinate directions.

Absolute Accuracy Test of the W100

The W100 gives better theoretical precision and empirical accuracy values than the N93 (versions 33 and 34 in Table II). The standard deviation of image observations is in the same range as with the N93, one quarter of a pixel. The W100 reveals residual error magnitude similar to those of the N93 (Fig. 7(e) and (f)).

TABLE II. Absolute accuracy test of the K750i (versions 10 to 14), N93 (versions 23 and 24), W100 (versions 33 and 34) and F828 (versions 43 and 44).

ver	*gcp*	*chk*	*tie*	*ap*	*rej*	σ_0	*std-X*	*std-Y*	*std-Z*	*rmse-X*	*rmse-Y*	*rmse-Z*
						µm	***of chk + tie points (mm)***			***at chk points (mm)***		
						pixel	*of only gcp points (mm)*			*at gcp points (mm)*		
10	87	0	90	10	0	**1·20**	**0·291**	**0·558**	**0·251**	n/a	n/a	n/a
						0·43	0·109	0·182	0·107	0·086	0·125	0·053
11	87	0	80	10	26[1]	**0·65**	**0·187**	**0·307**	**0·161**	n/a	n/a	n/a
						0·23	0·026	0·039	0·026	0·006	0·008	0·005
12	87	0	80	44	26[1]	**0·64**	**0·185**	**0·304**	**0·159**	n/a	n/a	n/a
						0·23	0·025	0·038	0·025	0·006	0·008	0·005
13	10	77	80	10	27[1]	**0·61**	**0·196**	**0·318**	**0·173**	**0·499**	**1·048**	**0·501**
						0·22	0·024	0·036	0·024	0·008	0·012	0·005
14	167	–	–	10	30[1]	**0·59**	**0·174**	**0·283**	**0·151**	n/a	n/a	n/a
	free					0·21	n/a	n/a	n/a	n/a	n/a	n/a
23	10	77	99	10	0	**0·50**	**0·161**	**0·284**	**0·140**	**0·701**	**0·816**	**0·203**
						0·23	0·047	0·077	0·046	0·036	0·101	0·030
24	186	–	–	10	0	**0·47**	**0·144**	**0·250**	**0·120**	n/a	n/a	n/a
	free					0·21	n/a	n/a	n/a	n/a	n/a	n/a
33	10	77	92	10	0	**0·47**	**0·100**	**0·168**	**0·085**	**0·501**	**0·421**	**0·443**
						0·21	0·022	0·035	0·021	0·049	0·078	0·050
34	179	–	–	10	0	**0·44**	**0·083**	**0·140**	**0·067**	n/a	n/a	n/a
	free					0·20	n/a	n/a	n/a	n/a	n/a	n/a
43	10	77	81	10	0	**0·26**	**0·049**	**0·084**	**0·043**	**0·097**	**0·144**	**0·134**
						0·10	0·022	0·036	0·022	0·055	0·033	0·022
44	168	–	–	10	0	**0·25**	**0·043**	**0·074**	**0·037**	n/a	n/a	n/a
	free					0·09	n/a	n/a	n/a	n/a	n/a	n/a

ver : version number.
gcp/chk/tie : number of control points/independent check points/tie points, respectively.
ap : number of additional parameters.
rej : rejected rays by data snooping, rejection rule for[1] : reject all residuals $\geq 4\sigma_0$.
σ_0 : standard deviation of image observations a posteriori.
std : average theoretical precision values of *chk/tie/gcp* coordinates.
rmse : empirical accuracies of *chk/gcp* coordinates.

Absolute Accuracy Test of the F828

The F828 gives the best performance and remarkably superior numbers compared to the other cameras (versions 43 and 44 in Table II). The value of σ_0 goes down to 1/10 of a pixel, satisfying the theoretical expectations of the least squares template matching. Also, the empirical rmse are in much better agreement with the theoretical standard deviations.

More information covering other computational versions of all four cameras can be found in Gruen and Akca (2008b).

The systematic deviations from the ideal camera model, in other words, the symmetric radial and asymmetric decentring lens distortions, are shown in Fig. 8. The affinity and the shear are not plotted, since their total effect is less than 1 µm.

Note that two cameras equipped with a Carl Zeiss Vario-Tessar lens, the N93 and the W100, have similar magnitudes for the decentring lens distortion. Large shift values of the principal point locations of the N93 and W100 were identified. The estimated principal point locations are given in Table III where the large numbers can be attributed to imperfect mounting of the lenses and/or the chips.

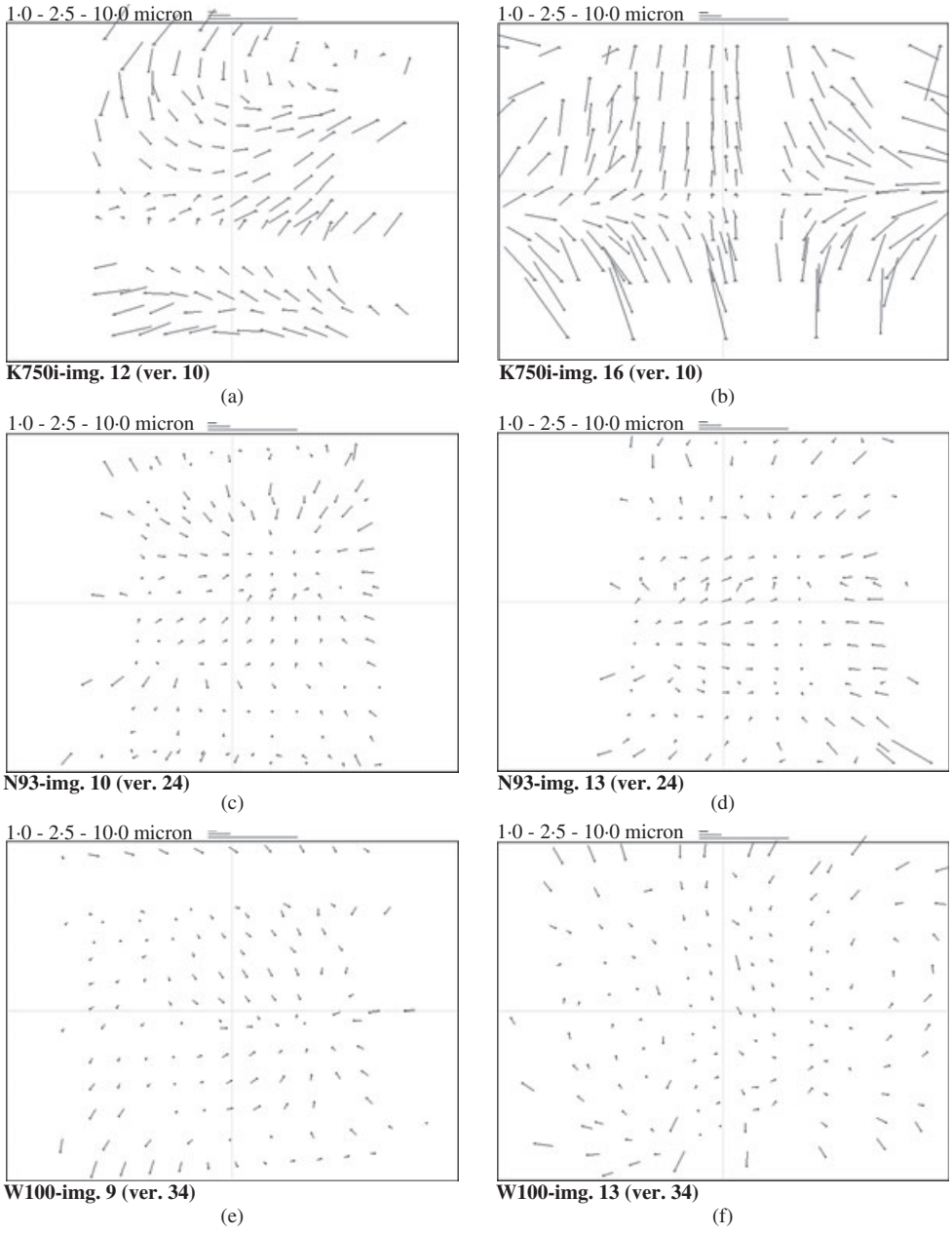

FIG. 7. Systematic residual patterns of the K750i, N93 and W100 after the self-calibrating bundle adjustment.

In spite of giving the largest radial lens distortion (approaching 275 μm at the corners), the F828 is the best camera considering the absolute accuracy tests given here and in the previous

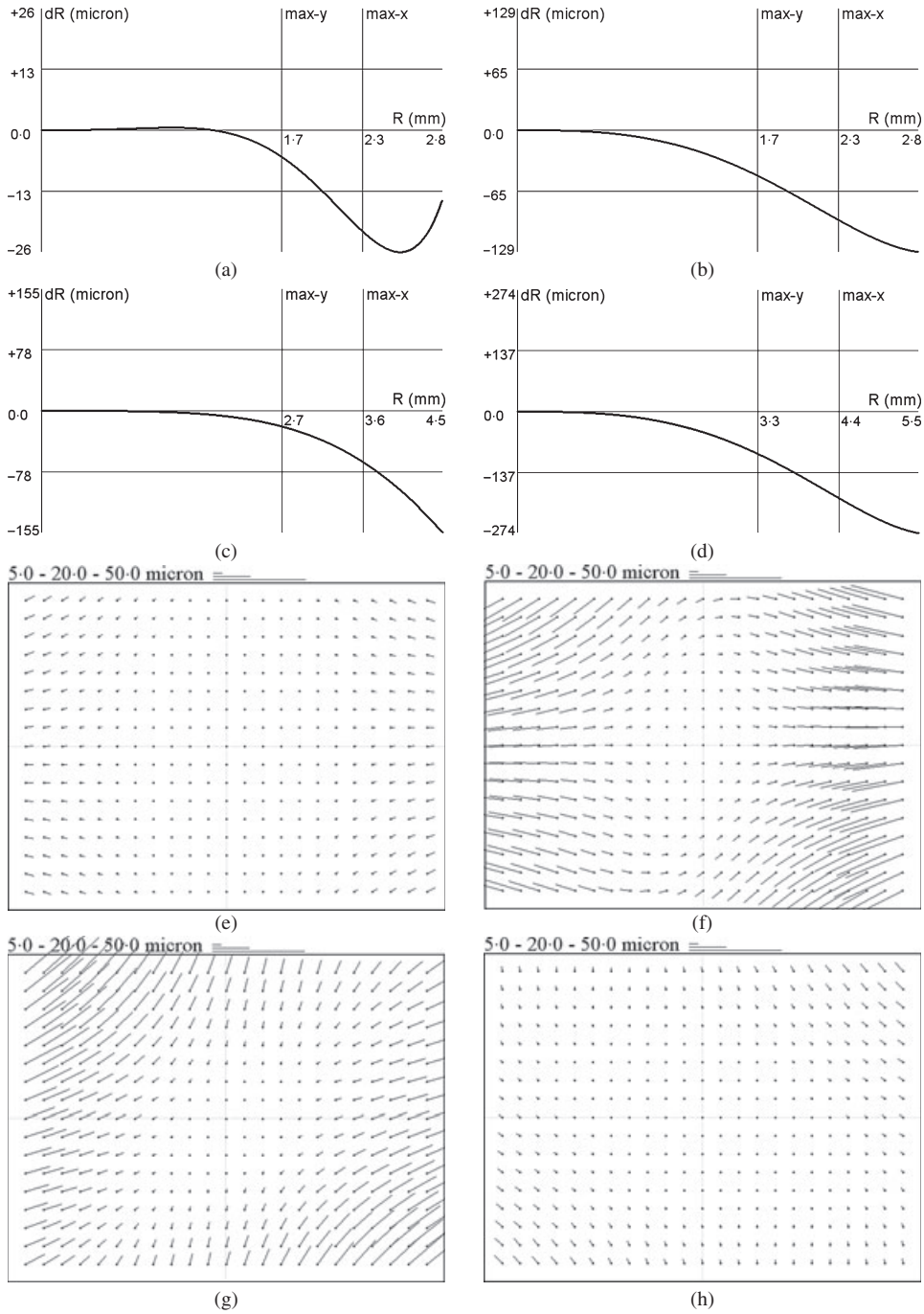

FIG. 8. (a), (b), (c), (d) Radial lens distortion profiles of the K750i, N93, W100 and F828, respectively. (e), (f), (g), (h) Decentring lens distortion plots of the K750i, N93, W100 and F828, respectively. The graphics represent the computational results of versions 14, 24, 34 and 44.

TABLE III. Principal point offsets in the various cameras.

Camera	*Version number*	x_0 (μm)	std-x_0 (μm)	y_0 (μm)	std-y_0 (μm)
K750i	Version 14	+31·9	1·2	−49·8	0·9
N93	Version 24	−109·8	0·8	+14·8	0·7
W100	Version 34	+68·3	0·9	−159·2	0·8
F828	Version 44	−8·8	0·4	−27·6	0·3

TABLE IV. JPEG compression test with the F828 (*gcp*/*chk*/*tie* are 44/43/81, respectively).

ver	*Compression*	*ap*	*rej*	σ_0	*std-X*	*std-Y*	*std-Z*	*rmse-X*	*rmse-Y*	*rmse-Z*
				μm *pixel*	***of chk + tie points (mm)*** *of only gcp points (mm)*			***at chk points (mm)*** *at gcp points (mm)*		
51	Original	10	0	**0·26**	**0·047**	**0·082**	**0·040**	**0·077**	**0·120**	**0·059**
	TIFF, 22·9 MB			0·10	0·022	0·036	0·022	0·034	0·033	0·028
52	5·5	10	0	**0·26**	**0·047**	**0·082**	**0·040**	**0·078**	**0·124**	**0·059**
	Q100, 4·2 MB			0·10	0·022	0·036	0·022	0·034	0·033	0·027
53	41·6	10	0	**0·26**	**0·047**	**0·082**	**0·040**	**0·077**	**0·132**	**0·060**
	Q70, 0·5 MB			0·10	0·022	0·036	0·022	0·033	0·033	0·028

sub-sections. Conversely, the K750i gives the smallest magnitudes for the radial and decentring lens distortions, but the worst results in the absolute accuracy tests.

JPEG Test with the F828

The use of JPEG images for the image measurements of the K750i, N93 and W100 and the observed image-variant residual error patterns raised the question whether the JPEG compression has an effect on the results. The original TIFF images of the F828 were converted to quality level 100 (maximum quality) and 70 JPEG images, using the free software IrfanView (version 3.98, http://www.irfanview.com/) and subjected to accuracy testing. Table IV gives the results. The loss of empirical accuracy due to ∼42 times JPEG compression is only 12 μm in depth (versions 51 and 53 in Table IV). The other coordinates are of the same accuracy as with the TIFF images. The results are in disagreement with those given in Lam et al. (2001), Li et al. (2002) and Shih and Liu (2005). However, their tests are on aerial images, whereas this project used a close range test object under good illumination conditions.

Temporal Stability Test with the N93

In order to check the temporal stability of the interior orientation over time, two sets of images of the N93 were acquired, the first data-set on 6th February 2007 (Table II) and the second on 30th September 2007 (Table V). Both data-sets have the same number of images taken at roughly the same locations.

The September 2007 data-set has slightly better theoretical precision and empirical accuracy numbers than the February 2007 results. This is because of slightly better convergent image acquisition geometry of the September 2007 data-set. Similar residual systematic error patterns (after self-calibration with block-invariant additional parameters) as before (February 2007) were also found on the September 2007 images (compare Fig. 7(c) and (d) with Fig. 9(a) and (b)).

TABLE V. Temporal stability test of the N93 (image acquisition on 30th September 2007).

ver	*gcp*	*chk*	*tie*	*ap*	*rej*	σ_0	*std-X*	*std-Y*	*std-Z*	*rmse-X*	*rmse-Y*	*rmse-Z*
						μm *pixel*	***of chk + tie points (mm)*** *of only gcp points (mm)*			***at chk points (mm)*** *at gcp points (mm)*		
63	10	77	99	10	0	**0·49**	**0·155**	**0·245**	**0·136**	**0·574**	**0·636**	**0·222**
						0·22	0·047	0·076	0·046	0·021	0·066	0·017
64	186 free	–	–	10	0	**0·48**	**0·138**	**0·217**	**0·116**	n/a	n/a	n/a
						0·22	n/a	n/a	n/a	n/a	n/a	n/a

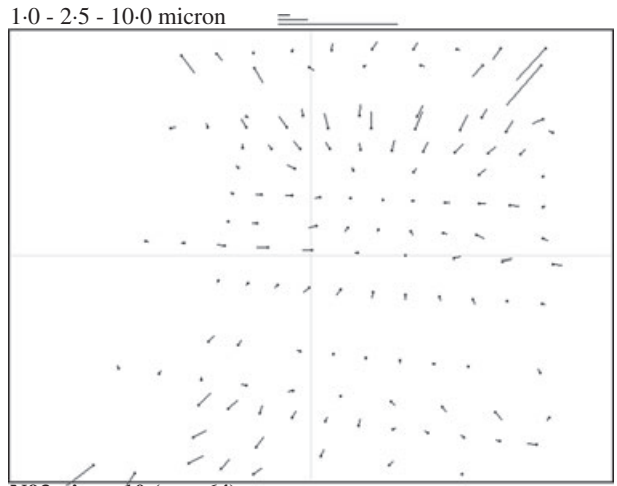

(a)

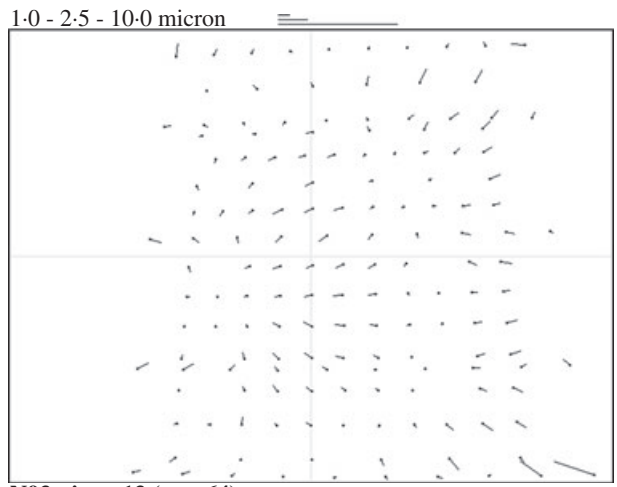

(b)

FIG. 9. Systematic residual patterns of images number 10 (a) and number 13 (b) of version 64 (September 2007 epoch of the N93) after the self-calibrating bundle adjustment.

The tie point coordinates of the version 23 (February 2007) and version 63 (September 2007) results were compared. The means of the differences (February 2007 to September 2007) are +0·109, +0·148 and +0·047 mm for the *X*, *Y* and *Z* axes, respectively. The standard deviations of the coordinate differences (±0·141, ±0·214 and ±0·133 mm for the *X*, *Y* and *Z* axes, respectively) are considerably smaller than the empirical accuracy numbers.

The changes in the principal point locations (x_0 and y_0) and the focal length (c) between version 24 (February 2007) and version 64 (September 2007) are only −1·7, +1·4 and −1·1 μm, respectively. The corresponding standard deviations of the differences (calculated according to the law of error propagation without considering the correlations) are ±1·1, ±0·9 and ±0·9 μm, respectively. In order to understand longer term trends and anomalies, more temporal data-sets may be needed.

Image Residual Analysis

In an image residual analysis, the directions and the magnitudes of the residual vectors at predefined grid locations (in the present case at 24 × 18 locations) were averaged. This shows the nature of the systematic errors remaining after the self-calibrating bundle adjustment (Fig. 10).

The systematic error pattern of the 12-image version (Fig. 10(b)) of the K750i is in parts similar to the 18-image version (Fig. 10(a)). It was also noted that the image residual analysis results of the two epochs' calibration results of the N93 are almost identical (Fig. 10(c) and (d)).

The character of the mean residual patterns suggests that they cannot be compensated by the usual sets of self-calibration parameters. Also, up to now the physical causes of these kinds of error patterns are not understood.

The photo-invariant additional parameters were used in the literature mostly for the self-calibration at multiple focal settings (Fraser, 1980) and for analysing the camera body mounting instability (Shortis et al., 1998; Hastedt et al., 2002). Camera bodies of SLR type tend to be less stable than those of "compact" cameras (Shortis et al., 1998; Wackrow et al., 2007). In these tests photo-invariant additional parameters have also been applied. They also did not fully compensate the systematic error patterns, because these types of patterns cannot be covered by usual correction polynomials. Other functions have to be developed for that.

Radiometric Performance Tests

The Radiometric Test Set-up

The same cameras were used for the radiometric analysis except for the W100, which was damaged just after the geometric tests. It was replaced with a Sony DSC T100 off-the-shelf camera, which is identical to the W100 in terms of sensor type, image format and lens (Fig. 11). It should be noted that, of the four cameras, only the T100 has an image stabiliser. Camera settings are important parameters for the radiometric performance tests. They are given in Table VI. Since the settings of the K750i and N93 cannot be changed by the user, the T100 and the F828 were allowed to make their settings automatically.

The Siemens Star chart was used for all the radiometric testing tasks (Fig. 12). The chart contains 144 sinusoidal cycles in a radial structure and has a size of 290 mm × 270 mm. The four black patches (at the corners) with a small white square inside are used to automatically detect the position of the Siemens Star. The star is surrounded by 16 linearly ramped grey level patches (Fig. 12). The sinusoidal cycles are used for the MTF computation and the ramped grey patches are used for the noise and the operating range analysis. The Siemens Star chart

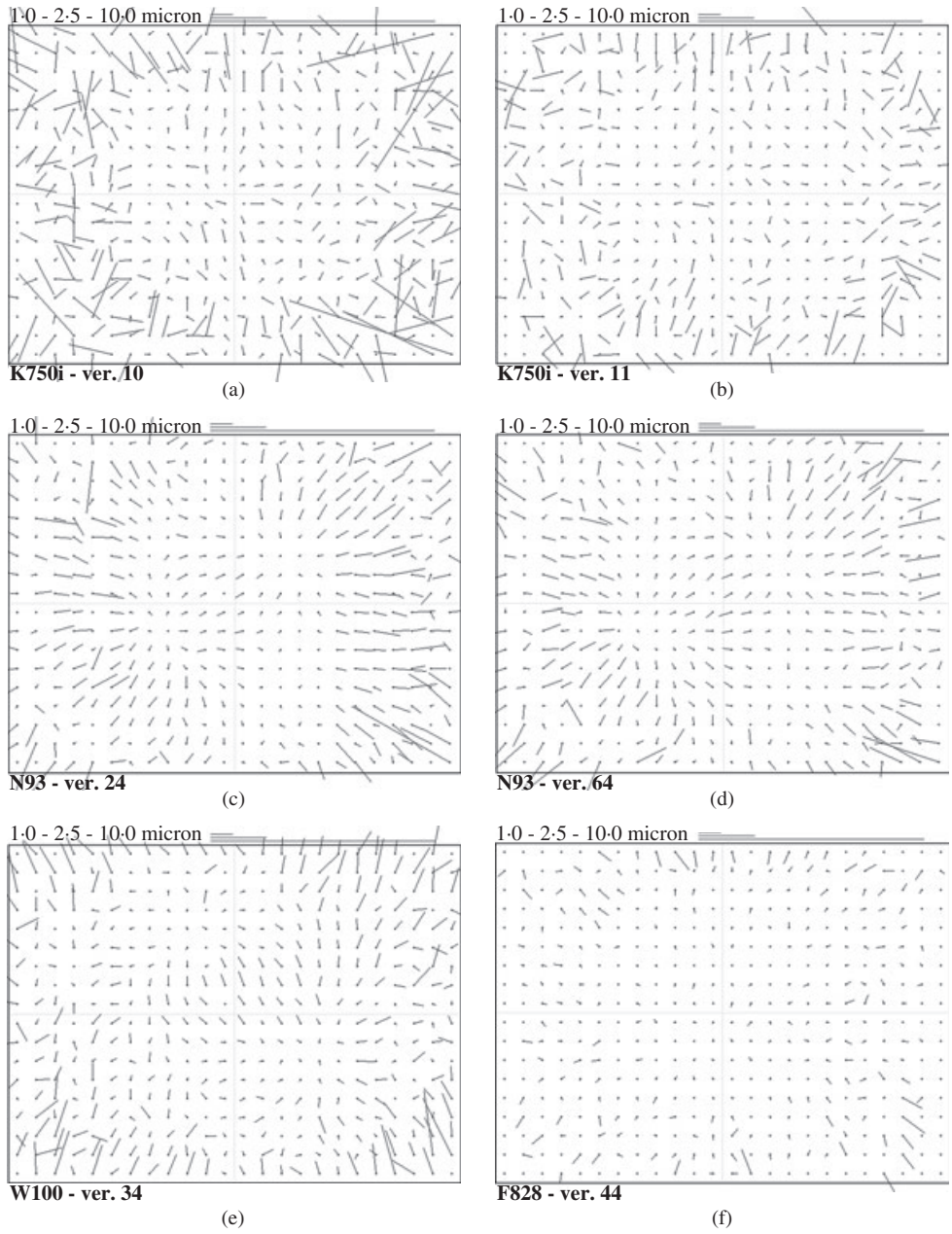

FIG. 10. Image residual analysis of the K750i, N93, W100 and F828, based on residual averaging over all images of a particular test configuration.

	T100
Sensor type	CCD
Sensor size	5·8 mm × 4·3 mm
Pixel size	1·8 μm
Image format	3264 × 2448 (8 Mpixel)
Lens	Carl Zeiss Vario-Tessar
Focal length	5·8 to 29·0 mm
Optical zoom	5×
Auto focus	Yes
Aperture	f/3·5 to 4·4
Output format	JPEG only

FIG. 11. Sony DSC T100.

TABLE VI. Exposure settings of the cameras.

	K750i	*N93*	*T100*	*F828*
Shutter speed	1/32	1/40	1/40	1/30
Lens aperture	f/2·8	f/3·3	f/3·5	f/2·0
ISO speed	ISO100	Unknown	ISO250	ISO64

and the associated software (only for the MTF computation) are provided by Image Engineering, Frechen, Germany (http://www.image-engineering.de). The algorithmic details of the approach are given in Loebich et al. (2007).

The camera resolution (based on the MTF analysis) was investigated at nine image locations by aligning the chart in three columns and three rows (Fig. 12). The pictures were taken at short object-to-camera distances in order that the camera field of view (FOV) just covered the 3 × 3 grid (Fig. 12). Thus, the computed MTF values are rather for comparative purposes. The pictures from all four cameras were taken at around the same time, under the same illumination conditions and using the same set-up. The focal lengths were set to the smallest values, which give the widest angles of the FOV. The cameras were fixed on a tripod to minimise motion blur.

Resolution Test by MTF Analysis

Image resolution is related to the ability of a camera to reproduce fine details. The MTF is a fundamental criterion for measuring the sharpness or spatial resolution performance of the imagery. It is mathematically defined as the normalised magnitude of the Fourier transform of the point spread function (PSF) or line spread function (LSF) of an imaging system.

The IE-Resolution-Single software (Image Engineering) divides each star into eight segments (Fig. 13(a)). Each segment is computed individually. The modulation at each

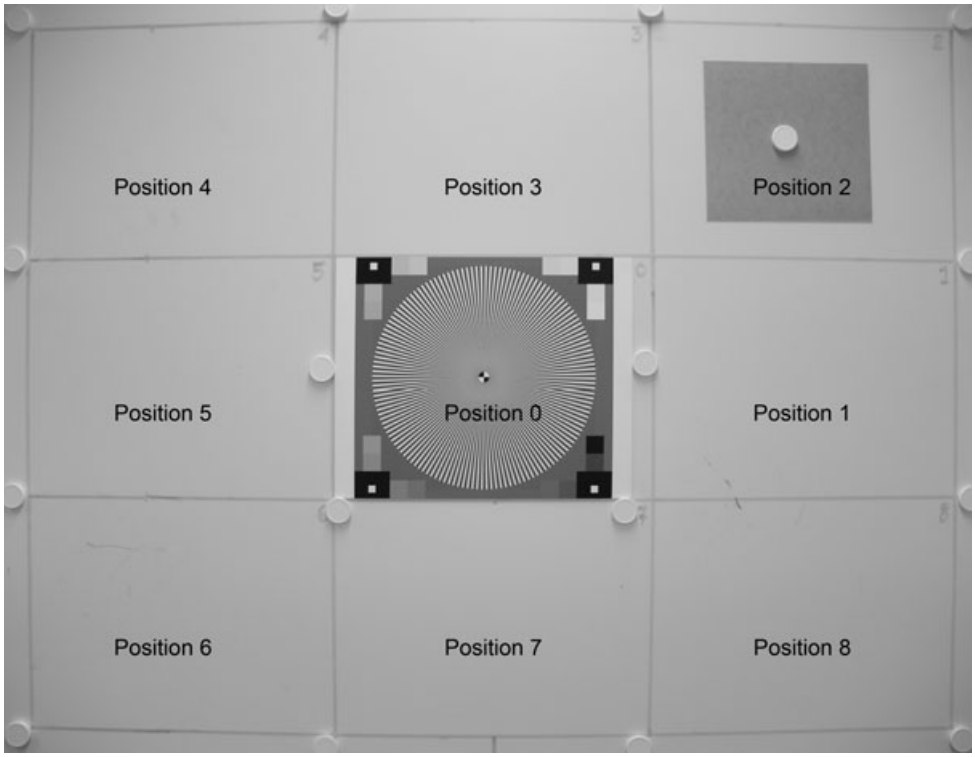

FIG. 12. The Siemens Star chart is located at nine positions of the image. The chart contains 16 linearly ramped grey patches that are located next to the black patches at the corners. This picture shows position 0 in the K750i image.

frequency is determined and the MTF curve is plotted as modulation against spatial frequency (Fig. 13(b) and (c)). The software gives the resolution in line pairs per picture height (LP/PH), which is later converted into line pairs per mm (lp/mm) by taking into account the sensor sizes (Table I and Fig. 11).

A 40% contrast (or modulation) was set as the MTF limit value. The results are given in Figs. 14–17 as spider diagrams. In Table VII the statistical results are given based on minimum, maximum, standard deviation and mean of the actual resolutions computed over all 72 segments.

The K750i gives the worst results (Fig. 14). The average resolution of all nine chart locations, considering all segments, is 88 lp/mm. Furthermore, the resolution is heterogeneous over the image format, worst at the lower left area and best at the upper right area. The change of the resolution from the upper right corner (103 lp/mm) to the lower left corner (73 lp/mm) is significant.

The MTF results for the N93 (Fig. 15) are slightly better than those for the K750i in terms of average resolution (96 lp/mm). However, the resolution values are again not homogeneous and isotropic over the chart locations and segment directions in image space. The average resolution value at the upper left corner is minimal (63 lp/mm), while the upper right corner has the best value (124 lp/mm). The maximum change of the resolution inside the image plane is by a factor of 3.

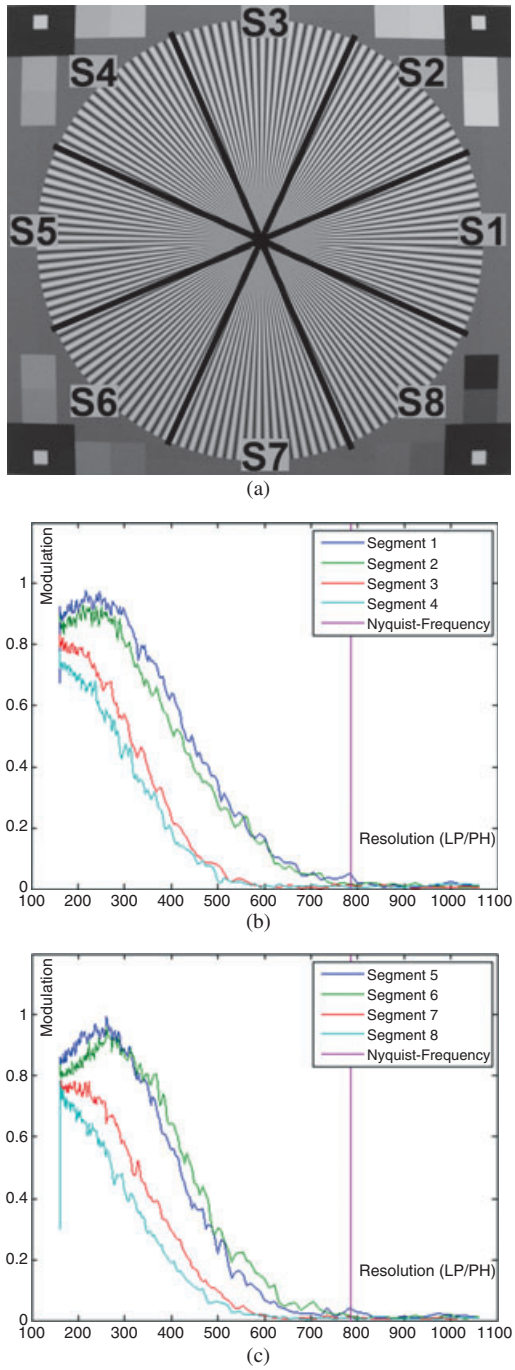

FIG. 13. The software computes the MTF graphs at eight segments of the chart. (a) The eight segments, (b) and (c) computed MTF graphs for all eight segments.

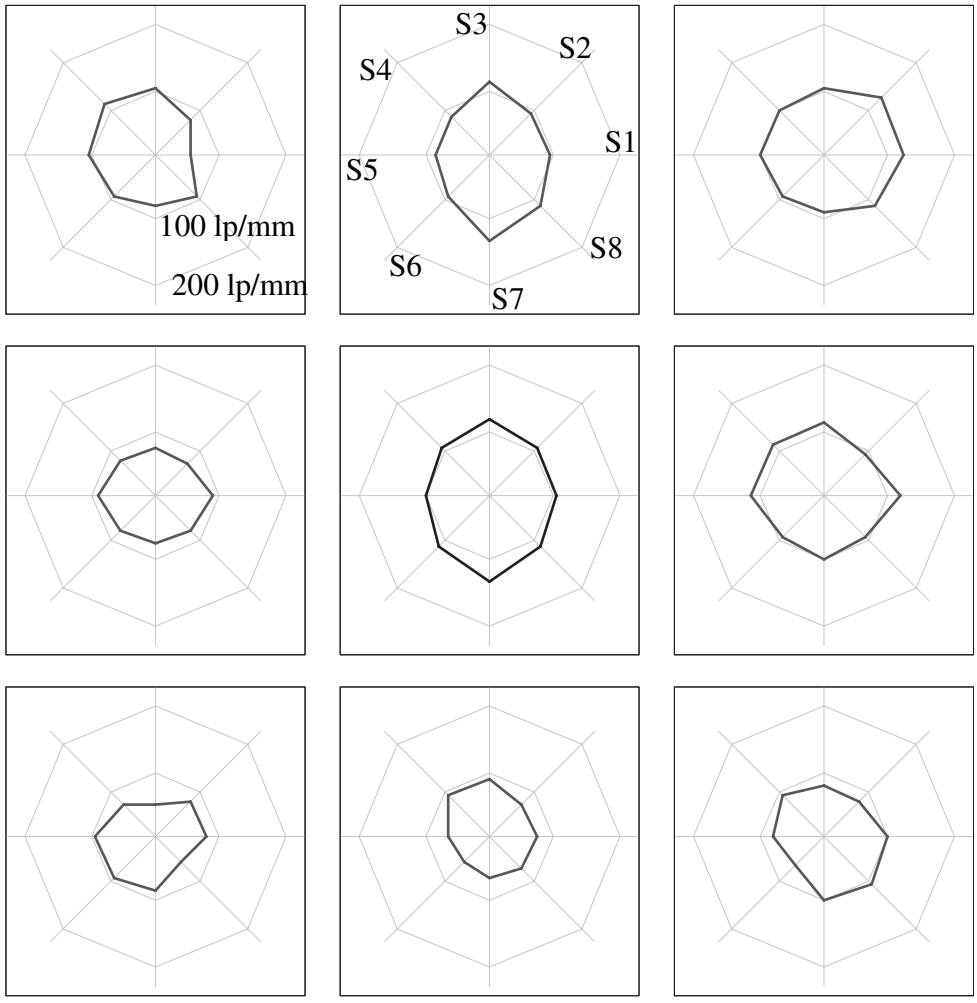

FIG. 14. Resolutions at all nine Siemens Star chart locations (according to Fig. 12) for the K750i. Each location contains the results of eight directional segments (S1, S2, …, S8). The internal octagon of the spider diagrams stands for 100 lp/mm and the external stands for 200 lp/mm. The same notation is also used for Figs. 15, 16 and 17.

The T100 (Fig. 16) gives the best average resolution (132 lp/mm) in terms of magnitude. This is in agreement with the nominal spatial resolution numbers given in Table VII. Although the F828 (Fig. 17) has a smaller mean value (96 lp/mm) than the T100, it is the best among these cameras in terms of homogeneity and isotropy.

Noise Analysis

The noise was analysed as a function of image intensity, as the noise variation for the CCD/CMOS sensors is intensity-dependent rather than simply additive (Zhang, 2005). The 16

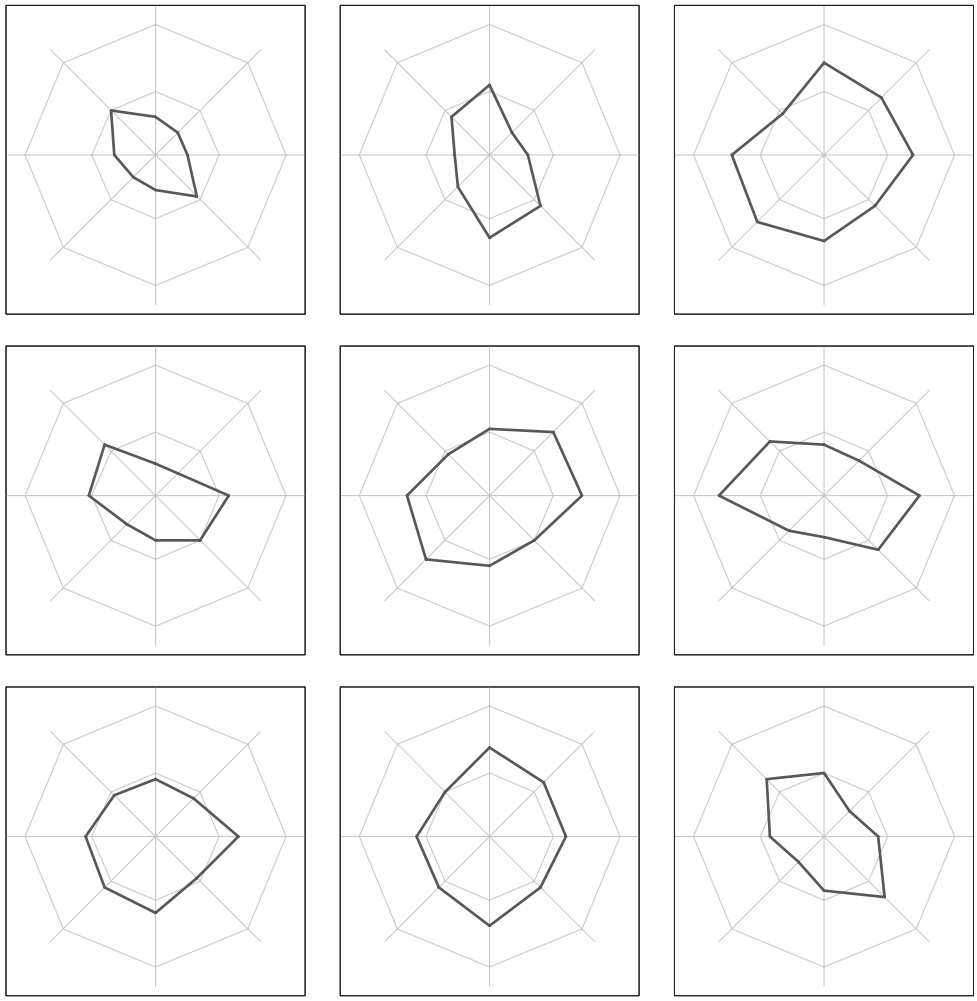

FIG. 15. Resolutions for the eight segments of all nine chart positions of the N93.

linearly ramped grey patches were used for this purpose. The patches are coded, starting from full black as L0 to full white as L15 (Fig. 12).

For the four cameras, the images at position 0 (Fig. 12) are used for the computations. At 16 ramped grey patches, the means and the standard deviations of the grey levels for each channel (red, green, blue) are calculated. The standard deviations show the noise characters of the cameras (R_{noise}, G_{noise} and B_{noise} columns in Table VIII).

The trends in Fig. 18 show a dependency of the noise on the image intensity, revealing higher noise content for the low grey value ramps.

The dynamic range (or operating range) is an important parameter in image noise estimation. Thus the signal-to-noise ratio (SNR) is a more representative indicator than the noise estimation alone. The SNR value for the red channel was estimated as follows:

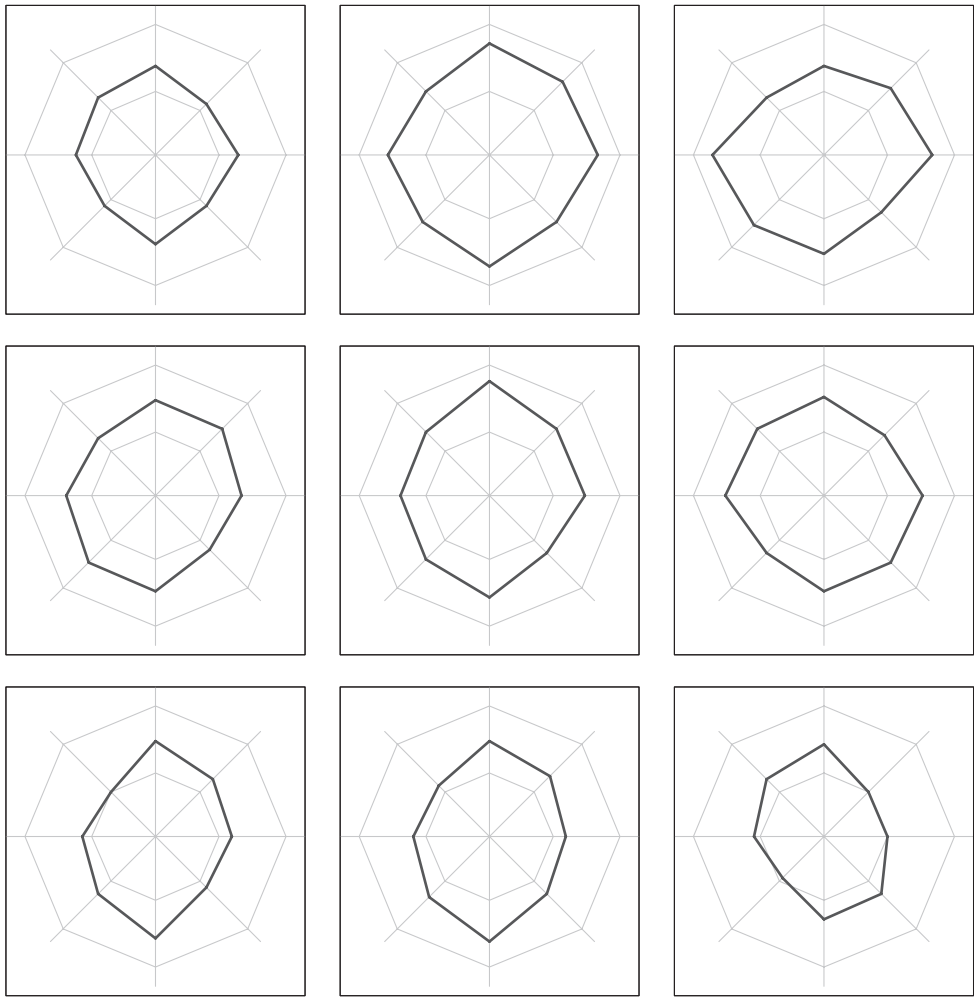

FIG. 16. Resolutions for the eight segments of all nine chart positions of the T100.

$$R_{SNR} = (R_{max} - R_{min})/R_{noise} \quad (1)$$

where R_{max} and R_{min} are the maximum (the mean of the white patch L15) and the minimum (the mean of the black patch L0) grey levels and R_{noise} is the estimated standard deviation. Equation (1) is used similarly for the green and blue channels as well.

The estimated noise of the K750i is smaller than the N93 and the T100 (Fig. 18). The reason might be that the K750i has a larger pixel size (2·8 μm), which should theoretically give less noise. Noise depends on the chip design and the data processes.

In terms of the SNR results, the T100 is clearly better than both of the mobile phone cameras because of its larger operating range. However, the K750i still has a better SNR than the N93. The F828 gives the smallest noise level and the best SNR value (Table VIII).

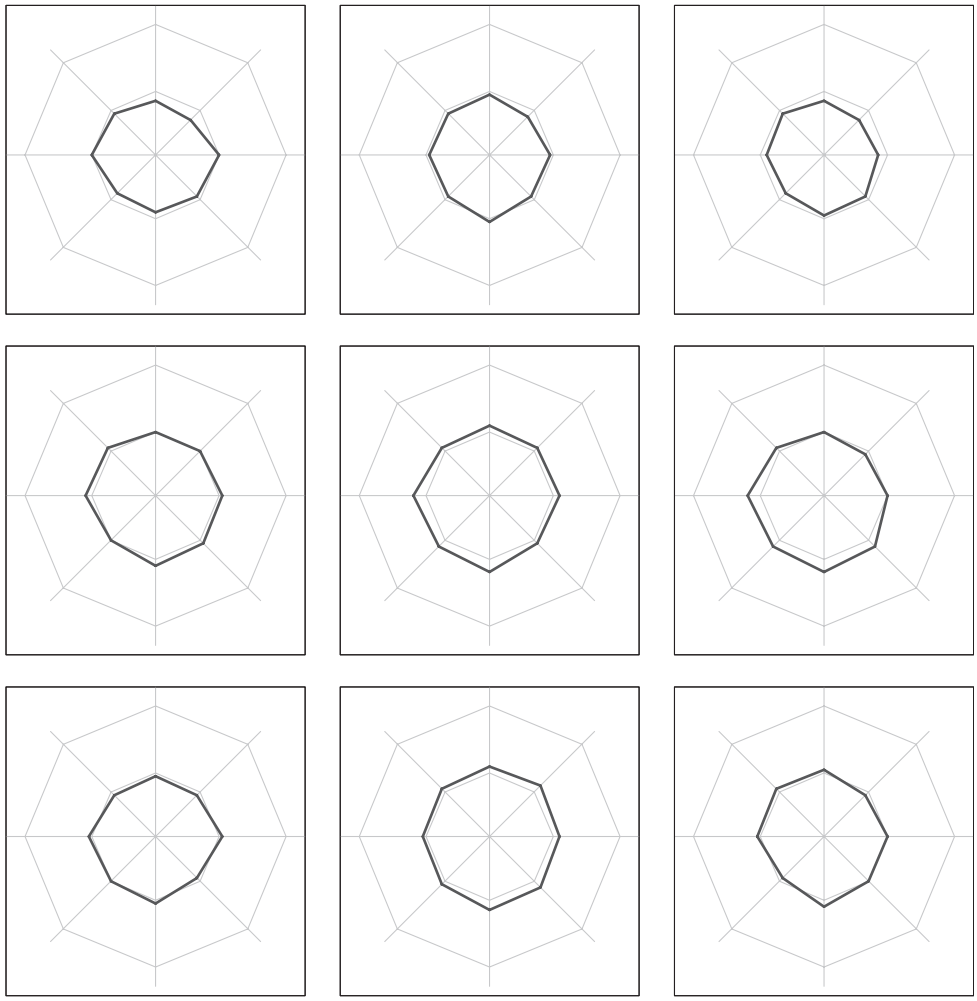

FIG. 17. Resolutions for the eight segments of all nine chart positions of the F828.

Operating Range Analysis

The linearity of response and the noise level are the parameters described over the dynamic range of an imaging system. In spite of the fact that the dynamic range test is critical for any radiometric analysis procedure, it cannot be determined correctly since the raw read-out values at the chip level are not disclosed to the user (except for the F828 whose SRF output format contains the raw image data). The K750i, N93 and T100 capture the scene and convert the raw data into JPEG image format (most probably together with an image enhancement pre-processing) using the sRGB colour representation (Stokes et al., 1996), which is the most commonly used colour space for digital cameras.

Nevertheless, the operating range was tested, which is the grey level range described over the given output (JPEG) images. The mean values computed at 16 linearly ramped grey

TABLE VII. Numerical results of the MTF analysis.

	Nominal resolving power[1] *(lp/mm)*	*Min (lp/mm)*	*Max (lp/mm)*	*Std. dev. (lp/mm)*	*Mean (lp/mm)*
K750i	178	50	131	18	88
N93	227	49	157	29	96
T100	277	89	171	18	132
F828	185	69	115	9	96

[1]Based on the given physical pixel size (Table I and Fig. 11).

TABLE VIII. Numerical results of the noise analysis.

	R_{min}–R_{max}	G_{min}–G_{max}	B_{min}–B_{max}	R_{noise}	G_{noise}	B_{noise}	R_{SNR}	G_{SNR}	B_{SNR}
						Mean			***Mean***
K750i	63·4–176·4	63·7–175·0	62·9–171·2	2·0	1·9	2·7	56·5	58·6	40·1
						2·2			**51·7**
N93	10·7–166·2	12·2–171·0	12·0–173·7	3·2	2·8	4·2	48·6	56·7	38·5
						3·4			**47·9**
T100	19·0–205·3	19·5–194·9	17·7–178·1	2·4	1·8	2·9	77·6	97·4	55·3
						2·4			**76·8**
F828	17·6–198·2	21·1–204·2	24·0–197·0	1·8	1·5	2·0	100·3	122·1	86·5
						1·8			**103·0**

Mean noise = $(R_{noise} + G_{noise} + B_{noise})/3$.
Mean SNR = $(R_{SNR} + G_{SNR} + B_{SNR})/3$.

patches were used. They are drawn against their nominal values in Fig. 19. The comparative results show that the K750i has the smallest operating range in the image histogram. The K750i and N93, as mobile phone cameras, give smaller grey value ranges than the T100 and F828 off-the-shelf cameras.

Linearity

The brightness perceived by the human visual system is a logarithmic function of the incident light intensity. By contrast, the imaging systems are designed to be linear in radiometric response (at the chip level). Read-out values are converted to the standard image file formats using a colour representation model. The sRGB colour representation will somewhat disturb the linearity of the original raw image. Due to the fact that the raw image data (of the K750i, N93 and T100) cannot be accessed, a straightforward linearity test is not possible.

ANALYSIS OF RESULTS

The K750i, N93 and W100 cameras gave identical standard deviation values for image observations (between one quarter and one fifth of a pixel). They all apply a chip-level image enhancement for sharpening the images. This effect is visible in Fig. 5(a), (b) and (c). This low-level image enhancement, while improving the visual quality, is probably reducing the geometric quality of the cameras. They show noticeably block-variant systematic errors after the self-calibrating bundle adjustment with block-invariant additional parameters.

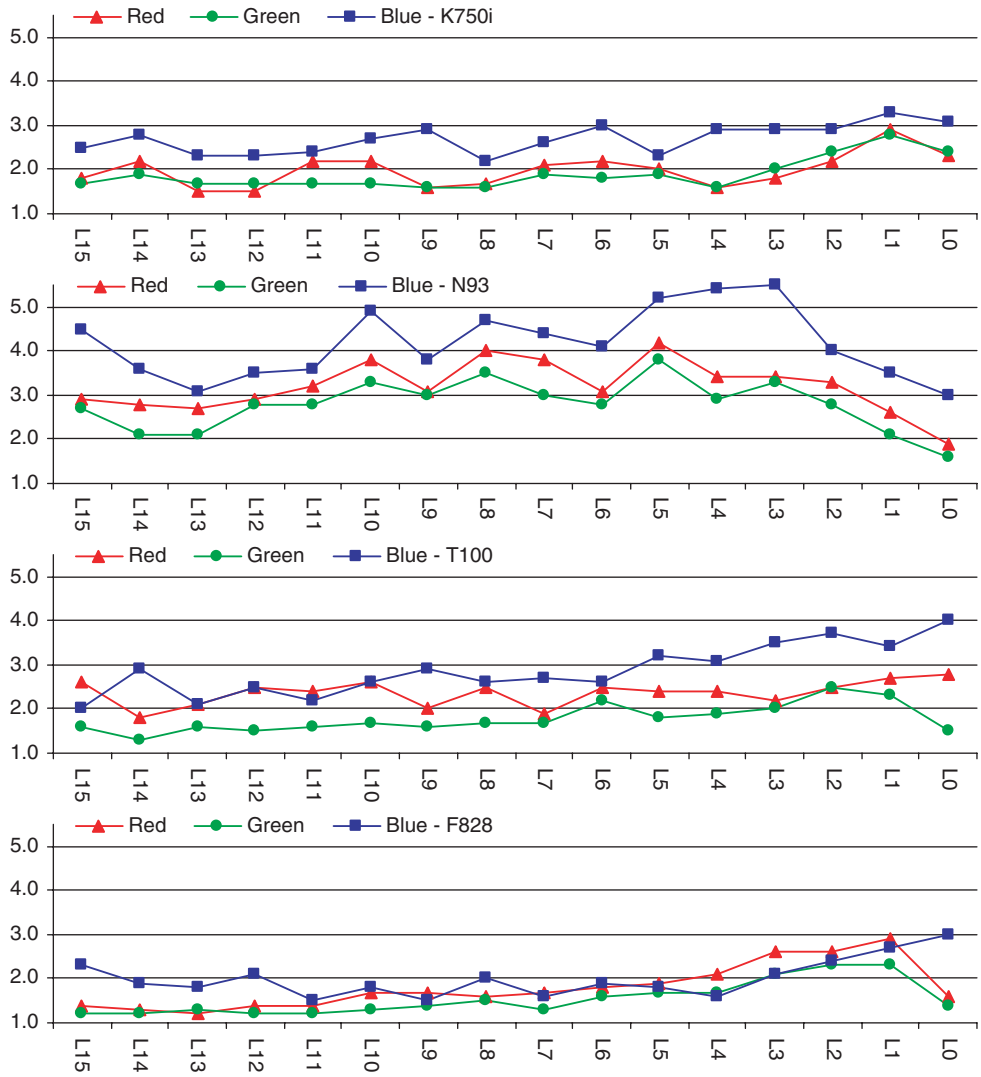

FIG. 18. Noise levels of the red, green and blue channels at 16 grey levels from white to black (L15, L14, …, L0). L15 stands for the white and L0 stands for the black colours. Ordinate values are standard deviation of the grey values. From top to bottom, the graphs stand for the K750i, N93, T100 and F828, respectively.

The self-calibration with photo-invariant additional parameters has also been applied, which again did not compensate the remaining systematic errors. These errors show a pattern which cannot be sufficiently modelled by the usual polynomial-based self-calibration functions.

In spite of giving the worst results in the test, the K750i can still offer millimetre-level accuracy in object space, although the block-invariant 10 and 44 AP sets cannot compensate fully for the systematic errors.

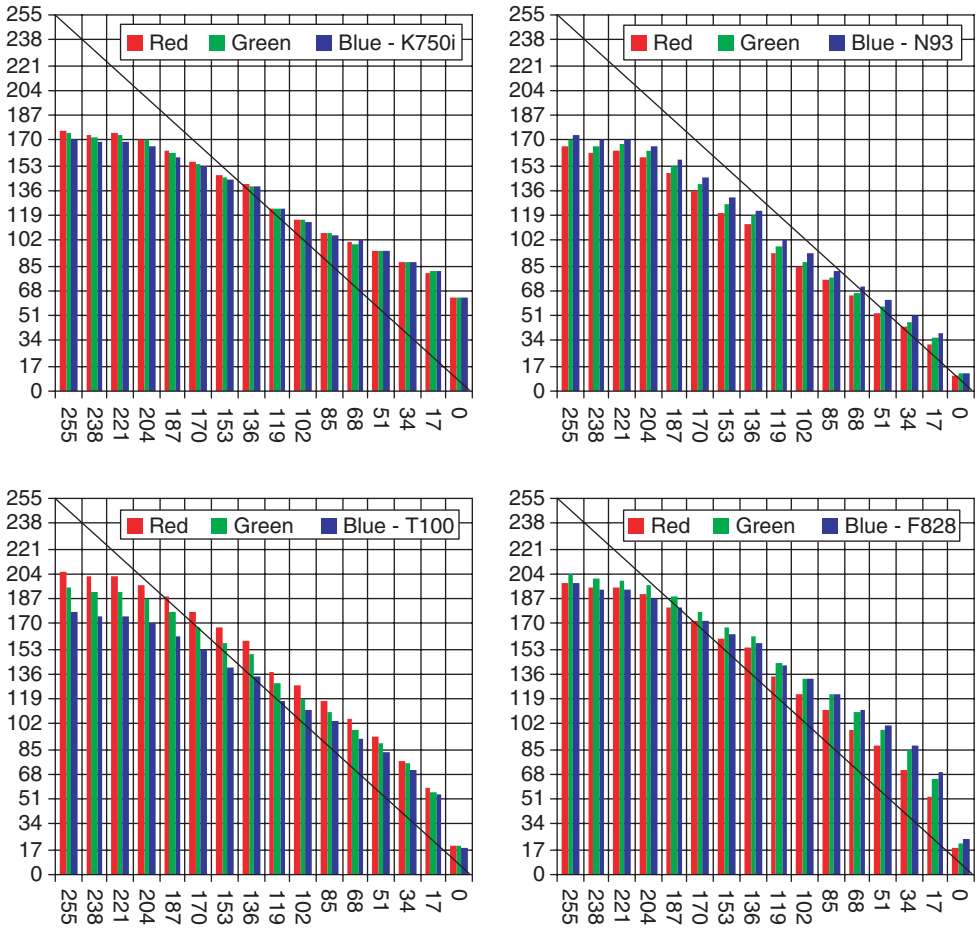

FIG. 19. Operating ranges of the K750i, N93, T100 and F828. Abscissa values are the nominal grey values of the 16 ramped grey patches (L0 = 0, L15 = 255). Ordinate values are the responses of the cameras in the 8-bit (0 to 255) grey value domain.

The N93 and W100 have the same lens systems (Zeiss Vario-Tessar). The W100 has a CCD sensor of larger size with 8 Mpixels. It is 2·5 times larger than the CMOS sensor of the N93. According to theoretical expectations, the N93 should give an accuracy of factor 1·6 (square root of 2·5) worse compared to the W100. The N93 almost strictly meets this expectation by giving 1·7 to 1·9 times worse results than the W100. On the other hand, there is a large difference between those two cameras, considering the size of the imaging system and the cost of the materials used in the construction. In this respect, the accuracy performance of the N93, as compared to the W100, is noteworthy.

Although the W100 and F828 have the same image format with 8 Mpixels, the expectation of equal accuracy does not hold here. The W100 gives substantially worse accuracy numbers (almost 3 times) than the F828. This is mainly due to a better lens system in the F828 and (possibly) to degradation resulting from the chip-level image enhancement operation of the W100.

The radiometric analysis shows that the radiometric performance of the mobile phone cameras is lower than that of the off-the-shelf digital cameras in terms of geometric resolution. However, given the large price difference between these two camera types, the overall performance of the mobile phone cameras is quite remarkable.

Conclusions

Metric calibration and metric accuracy tests were carried out on four consumer-grade imaging devices: two mobile phone cameras (Sony Ericsson K750i and Nokia N93) and two still video cameras (Sony DSC W100 and Sony DSC F828). The tests were performed using an in-house 3D testfield at ETH Zurich. Unwanted effects from image enhancement (sharpening) were found in the K750i, N93 and W100 cameras and JPEG compression artefacts in the N93. In all four cases, similar imaging geometry was used, under the same imaging conditions in order to make the results comparable.

With the given strong geometrical set-up, of course, all parameters for the interior orientation could be calibrated reliably.

The accuracy tests showed that in all cases the theoretical expectations, as indicated by the average standard deviations of the object space coordinates, could not be achieved by the empirical rmse figures computed from check points. The deviations ranged from a factor of 3·3 (K750i) to a factor of 1·7 (F828).

While the σ_0 values of the K750i, N93 and W100 are all at one fifth of a pixel level, they dropped down to one tenth of a pixel with the F828. This improvement in σ_0 is matched by the better behaviour of the post-adjustment image residuals. Only in the case of the F828 was there an almost random distribution. The other cameras, in particular the K750i, suffer from strong image-variant systematic errors. The block-invariant additional parameters could not compensate these errors. The error patterns are also not in agreement with what is usually encountered in photogrammetry. Therefore, standard additional parameter functions cannot compensate for these defects. So far, it has not been possible to explain the reasons for these errors. Could they lie in the image enhancement procedure, or any other shortcomings in the electronic circuits such as warm-up effects?

Nevertheless, and despite these problems, relative accuracies of 1:8000 in-plane and 0·03% of average depth were achieved with the K750i, and 1:34 000 in-plane and 0·005% of average depth with the F828, using in both cases 10 control points. This superior behaviour of the F828 can only partly be explained by the larger image format (8 Mpixels versus 2 Mpixels), which theoretically should only lead to an improvement by a factor of 2.

If a free network adjustment is applied to both cameras by minimising the trace of the covariance matrix for the object space coordinates, the following values are obtained: 1:25 000 and 0·009% for the K750i and 1:99 000 and 0·0025% for the F828. This shows roughly the same relationship between both cameras; however, it gives a better indication of the potential system accuracy. It is worth noting that, compared to the film-based large format aerial photogrammetric block adjustment accuracy, the same and better accuracies in height and almost the same in planimetry can be achieved here, if for the aerial case an object area of one image coverage only is considered (as in the close range case described in this paper). This definitely indicates the great potential of consumer-grade and even mobile phone cameras for photogrammetric processing. The main remaining problem is to find a convincing explanation for the image-to-image variation in systematic error pattern in some of the mobile phone cameras.

In a final test, the effect of JPEG compression on the metric system accuracy was also checked for the F828 camera. Even when going up to a factor of 42 compression rate, only a

small reduction in accuracy occurred (9% in the depth direction). This can be considered of little importance.

The tests of the N93 were spread over a longer time period in order to check the temporal stability of the calibration. It was observed that the interior orientation of the N93 did not change significantly according to the one-dimensional statistical test procedure employed.

The image quality studies show that the radiometric performances of the mobile phone cameras are lower than the still video cameras in terms of resolution, noise, signal-to-noise ratio and operating range. Nevertheless, their radiometric capabilities are still sufficient to collect thematic information through their imagery.

It is believed that with a proper calibration and data processing software performance these devices can be used for many photogrammetric tasks that require an accuracy of around 1:10 000. The integration of GPS receivers and motion sensors will further broaden their applicability. Also, it is to be expected that the quality and performance of the integrated cameras will further improve, together with the on-board processing functions. This may eventually allow such a device to be used as a stand-alone photogrammetric data acquisition and processing tool, at least for smaller projects.

In conclusion, it can be stated that mobile cameras do give a very interesting option for performing ''mobile photogrammetry'', in terms of accuracy, cost and flexibility. In a future study, these cameras will be applied for 3D object modelling.

ACKNOWLEDGEMENTS

The authors thank Mr Thomas Hanusch and Dr Timo Kahlmann (ETH Zurich, Switzerland) for helping with the geodetic measurements of the testfield, Dr Jafar Amiri Parian (ETH Zurich, Switzerland) for running his self-calibrating bundle adjustment software with 44 additional parameters and Mr Uwe Artmann (Image Engineering, Frechen, Germany) for helping with the use of ''IE-Resolution-Single'' software.

REFERENCES

AL-BAKER, O., BENLAMRI, R. and AL-QAYEDI, A., 2005. A GPRS-based remote human face identification system for handheld devices. *Proceedings of Wireless and Optical Communications Networks*. 606 pages: 367–371.

AYDAR, U., AVSAR, E. O. and ALTAN, O., 2007. Obtaining façade plan of a historical building with orthorectification of single images gathered by mobile phone and digital camera. *Proceedings of the XXI International CIPA Symposium, Athens, Greece*. 855 pages: 89–92.

BALTSAVIAS, E. P., HAERING, S., KERSTEN, T. and DAM, A., 1998. Geometric and radiometric evaluation of the DSW300 roll film scanner. *ISPRS Journal of Photogrammetry and Remote Sensing*, 53(4): 217–234.

BALTSAVIAS, E. P., PATERAKI, M. and ZHANG, L., 2001. Radiometric and geometric evaluation of Ikonos Geo images and their use for 3D building modelling. *Proceedings of the Joint ISPRS Workshop on High Resolution Mapping from Space 2001*. Hanover, Germany. 21 pages (on CD-ROM).

BEYER, H. A., 1992. *Geometric and radiometric analysis of a CCD-camera based photogrammetric close-range system*. Mitteilungen Nr. 51, Institute for Geodesy and Photogrammetry, ETH Zurich. 186 pages.

BROCK, G. C., 1968. A review of current image evaluation techniques. *Journal of Photographic Science*, 16(6): 241–249.

CHOWDHURY, A., DARVEAUX, R., TOME, J., SCHOONEJONGEN, R., REIFEL, M., DE GUZMAN, A., PARK, S. S., KIM, Y. W. and KIM, H. W., 2005. Challenges of megapixel camera module assembly and test. *Proceedings of 55th Electronic Components and Technology Conference*, 2. 1949 pages: 1390–1401.

CHUNG, Y., JANG, D., YU, W., CHI, S., KIM, K. and SOH, J., 2004. Distortion correction for better character recognition of camera-based document images. *SPIE*, 5578: 389–399.

CLEMENS, G., SANAHUJA, F. and BEAUGEANT, C., 2005. Audio-enhanced panoramic image capturing and rendering on mobile devices. *IEEE International Conference on Multimedia and Expo*. 1596 pages: 988–991.

Crespi, M., De Vendicti, L., Poli, D., Wolff, K., Colosimo, G., Gruen, A. and Volpe, F., 2008. Radiometric quality and DSM generation analysis of CartoSat-1 stereo imagery. *International Archives of the Photogrammetry, Remote Sensing and Spatial Information Sciences*, 37(3): 1349–1355.

Fraser, C. S., 1980. Multiple focal setting self-calibration of close-range metric cameras. *Photogrammetric Engineering & Remote Sensing*, 46(9): 1161–1171.

Gruen, A., 1985. Adaptive least squares correlation: a powerful image matching technique. *South African Journal of Photogrammetry, Remote Sensing and Cartography*, 14(3): 175–187.

Gruen, A., 2008. Reality-based generation of virtual environments for digital earth. *International Journal of Digital Earth*, 1(1): 88–106.

Gruen, A. and Akca, D., 2007. Mobile photogrammetry. *Dreiländertagung SGPBF, DGPF und OVG*, DGPF Tagungsband 16/2007: 441–451.

Gruen, A. and Akca, D., 2008a. Evaluation of metric performance of mobile phone cameras. *Proceedings of International Calibration and Orientation Workshop EuroCOW 2008*, Castelldefels, Spain. 10 pages (only on CD-ROM).

Gruen, A. and Akca, D., 2008b. Metric accuracy testing with mobile phone cameras. *International Archives of the Photogrammetry, Remote Sensing and Spatial Information Sciences*, 37(B5): 729–736.

Gruen, A. W., 1983. *A test strategy for high resolution image scanners*. Reports of the Department of Geodetic Science and Surveying, Ohio State University, Columbus, Ohio, USA. Report No. 350. 55 pages.

Grün, A., 1978. Progress in photogrammetric point determination by compensating of systematic errors and detection of gross errors. *International Archives of Photogrammetry*, 22(3): 113–140.

Hastedt, H., Luhmann, T. and Tecklenburg, W., 2002. Image-variant interior orientation and sensor modelling of high-quality digital cameras. *International Archives of the Photogrammetry, Remote Sensing and Spatial Information Sciences*, 34(5): 27–32.

Honkavaara, E., Jaakkola, J., Markelin, L. and Becker, S., 2006. Evaluation of resolving power and MTF of DMC. *International Archives of the Photogrammetry, Remote Sensing and Spatial Information Sciences*, 36(A1): 6 pages (on CD-ROM).

Koga, M., Mine, R., Kameyama, T., Takahashi, T., Yamazaki, M. and Yamaguchi, T., 2005. Camera-based Kanji OCR for mobile-phones: practical issues. *Proceedings of 8th International Conference on Document Analysis and Recognition*, 2. 1285 pages: 635–639.

Kohm, K., 2004. Modulation transfer function measurement method and results for the Orbview-3 high resolution imaging satellite. *International Archives of the Photogrammetry, Remote Sensing and Spatial Information Sciences*, 35(B1): 7–12.

Lam, K. W. K., Li, Z. and Yuan, X., 2001. Effects of JPEG compression on the accuracy of digital terrain models automatically derived from digital aerial images. *Photogrammetric Record*, 17(98): 331–342.

Lambers, K., Eisenbeiss, H., Sauerbier, M., Kupferschmidt, D., Gaisecker, T., Sotoodeh, S. and Hanusch, T., 2007. Combining photogrammetry and laser scanning for the recording and modelling of the Late Intermediate Period site of Pinchango Alto, Palpa, Peru. *Journal of Archaeological Science*, 34(10): 1702–1712.

Lenz, R. K. and Tsai, R. Y., 1988. Techniques for calibration of the scale factor and image center for high accuracy 3-D machine vision metrology. *IEEE Transactions on Pattern Analysis and Machine Intelligence*, 10(5): 713–720.

Li, Z., Yuan, X. and Lam, K. W. K., 2002. Effects of JPEG compression on the accuracy of photogrammetric point determination. *Photogrammetric Engineering & Remote Sensing*, 68(8): 847–853.

Loebich, C., Wueller, D., Klingen, B. and Jaeger, A., 2007. Digital camera resolution measurement using sinusoidal Siemens stars. *SPIE*, 6502: 65020N. 11 pages.

Markelin, L., Honkavaara, E., Peltoniemi, J., Suomalainen, J. and Ahokas, E., 2006. Radiometric evaluation of digital aerial cameras. *International Archives of the Photogrammetry, Remote Sensing and Spatial Information Sciences*, 36(B1): 6 pages (on CD-ROM).

Myung-Jin, C., 2005. Development of compact auto focus actuator for camera phone by applying new electromagnetic configuration. *SPIE*, 6048: 60480J. 9 pages.

Parikh, T. S., 2005. Using mobile phones for secure, distributed document processing in the developing world. *IEEE Pervasive Computing*, 4(2): 74–81.

Pateraki, M. and Baltsavias, E., 2002. Adaptive multi-image matching algorithm for the Airborne Digital Sensor ADS40. *Map Asia 2002. Proceedings of Asian Conference on GIS, GPS, Aerial Photography and Remote Sensing*. 6 pages (on CD-ROM).

Physorg, 2004. *Sharp Develops 2-Megapixel CCD Camera Module for Mobile Phones with New 2X Optical Inner Zoom Lens*. http://www.physorg.com/news1207.html [Accessed: 30th April 2007].

Physorg, 2005. *Sharp Develops Two New 3-Megapixel CCD Camera Modules for Mobile Phones*. http://www.physorg.com/news6096.html [Accessed: 30th April 2007].

PITTORE, M., CAPPELLO, M., ANCONA, M. and SCAGLIOLA, N., 2005. Role of image recognition in defining the user's focus of attention in 3G phone applications: the AGAMEMNON experience. *Proceedings of IEEE International Conference on Image Processing*, 3. 1303 pages: 1012–1015.

RIEGEL, T. B., 2005. MPEG-4-based 2D facial animation for mobile devices. *SPIE*, 5684: 55–62.

ROHS, M., 2004. Real-world interaction with camera phones. *Ubiquitous Computing Systems*. *LNCS*, 3598: 74–89.

SCOTT, F., 1968. The search for a summary measure of image quality. *Photographic Science and Engineering*, 12(3): 154–164.

SHIH, T.-Y. and LIU, J.-K., 2005. Effects of JPEG 2000 compression on automated DSM extraction: evidence from aerial photographs. *Photogrammetric Record*, 20(112): 351–365.

SHORTIS, M. R., ROBSON, S. and BEYER, H. A., 1998. Principal point behaviour and calibration parameter models for Kodak DCS cameras. *Photogrammetric Record*, 16(92): 165–186.

STOKES, M., ANDERSON, M., CHANDRASEKAR, S. and MOTTA, R., 1996. *A standard default colour space for the Internet: sRGB, Version 1.10*. http://www.color.org/sRGB.xalter [Accessed: 2nd March 2009].

UEDA, N., NAKANISHI, Y., MATSUKAWA, S. and MOTOE, M., 2004. Developing a GIS using a mobile phone equipped with a camera and a GPS, and its exhibitions. *Proceedings of 24th International Conference on Distributed Computing Systems Workshops*. 902 pages: 414–417.

WACKROW, R., CHANDLER, J. H. and BRYAN, P., 2007. Geometric consistency and stability of consumer-grade digital cameras for accurate spatial measurement. *Photogrammetric Record*, 22(118): 121–134.

WATANABE, Y., SONO, K., YOKOMIZO, K. and OKADA, Y., 2003. Translation camera on mobile phone. *Proceedings of International Conference on Multimedia and Expo*, 2. 639 pages: 177–180.

WELCH, R., 1971. Modulation transfer functions. *Photogrammetric Engineering*, 37(3): 247–259.

WELCH, R. and HALLIDAY, J., 1973. Imaging characteristics of photogrammetric camera systems. *Photogrammetria*, 29(1): 1–43.

WILLIAMS, M., 2006. CeBIT: Samsung shows 10-Megapixel camera phone. *PCWORLD*, 03/2009. http://www.pcworld.com/article/id,125020/article.html [Accessed: 30th April 2007].

ZHANG, L., 2005. *Automatic Digital Surface Model (DSM) generation from linear array images*. Mitteilungen Nr. 88, Institute for Geodesy and Photogrammetry, ETH Zurich. 219 pages.

Résumé

Cet article examine le potentiel des téléphones portables comme capteurs frontaux pour des procédures et des applications photogrammétriques. À cette fin, les caméras de deux téléphones portables (Sony Ericsson K750i et Nokia N93) ont été étalonnées sur notre dispositif d'étalonnage 3D en salle, en utilisant une compensation par faisceaux auto-étalonnante. Des tests de précision géométrique ont été effectués afin d'évaluer leur performance métrique et de la comparer à deux appareils photo numériques du commerce (Sony DSC W100 et Sony DSC F828). L'évaluation de la précision géométrique comprend un test de précision absolue, un test JPEG et un test de stabilité temporelle. Nous avons aussi évalué et comparé les performances radiométriques de toutes les caméras (excepté la caméra DSC W100 qui a été remplacée par la caméra DSC T100) par l'analyse de la fonction de transfert de modulation (FTM), l'analyse du bruit et un test d'autonomie. Dans certains systèmes, nous avons détecté des erreurs systématiques importantes. Toutefois, il semble que l'on puisse utiliser ces appareils pour de nombreux travaux photogrammétriques pour peu qu'ils aient été correctement étalonnés.

Zusammenfassung

Dieser Beitrag untersucht, inwieweit integrierte Handykameras zur Bilddatengewinnung in der Photogrammetrie nutzbringend eingesetzt werden können. Zu diesem Zweck kalibrierten wir die Kameras der Handys Sony Ericsson K750i und Nokia N93 unter Benutzung unseres 3D Testfelds und unter Einsatz des Verfahrens

der Selbstkalibrierung. Gleichzeitig benutzten wir das Testfeld für Genauigkeitsstudien. Wir bestimmten die metrischen Qualitäten dieser Kameras und verglichen diese mit denen dreier handelsüblicher Stillvideo-Kameras. Dieses beinhaltete einen Test auf absolute 3D Genauigkeit im Objektraum, die Untersuchung des Einflusses der JPEG Komprimierung und einen Test auf zeitabhängige Stabilität. Wir bestimmten das radiometrische Verhalten aller Kameras, indem wir die MTF, das Bildrauschen und die Linearität analysierten. In einigen dieser Kameras haben wir signifikante systematische Fehler diagnostiziert, die sich nicht mit den üblichen globalen Funktionen block-invarianter zusätzlicher Parameter kompensieren lassen. Dennoch erhielten wir mit diesen Handykameras erstaunlich gute Genauigkeiten. Sie eignen sich somit nach erfolgter Kalibrierung sehr wohl zum Einsatz in einer Vielzahl photogrammetrischer Anwendungen.

Resumen

Este artículo evalúa la capacidad de los teléfonos móviles para ser utilizados como sensores en aplicaciones y procedimientos fotogramétricos. Con este objetivo, se calibraron dos cámaras de teléfonos móviles (Sony Ericsson K750i y Nokia N93) en un campo de pruebas tridimensional interior, mediante un ajuste de haces con autocalibración. Las pruebas de exactitud geométrica se realizaron para evaluar su comportamiento métrico y para comparar los resultados con los de dos cámaras estacionarias de vídeo comerciales (Sony DSC W100 y Sony DSC F828). La evaluación de la exactitud geométrica consistió en una prueba de exactitud absoluta, prueba JPEG y prueba de estabilidad temporal. Se estimaron también las capacidades radiométricas de todas las cámaras (a excepción de la DSC W100 que fue sustituida por la cámara DSC T100) y se compararon mediante un análisis de la función de transferencia de modulación (FTM), un análisis del ruido de la imagen y del rango de operación. Se identificaron varios errores sistemáticos sustanciales en algunos equipos. Sin embargo, se confía en que, con una apropiada calibración, estos dispositivos puedan ser utilizados en muchas tareas fotogramétricas.

